Two-photon luminescence of gold nanorods: applications to single-particle tracking and spectroscopy

Carozza, S.

Chapter 3

Delivery and single-particle tracking of gold nanorods in live cells

Gold nanorods are promising labels for two-photon single-particle tracking in live cells, due to their brightness, stability and the use of low-energy photons, which reduces photodamage. We acquired 3D movies of gold nanorods in cells using a two-photon multifocal scanning microscope. We tested delivery of gold nanorods with different techniques: incubation, electroporation, cell-squeezing and single-cell microinjection in HeLa and COS1 cells, and injection in the yolk of zebrafish embryos cells. For each technique we evaluated the delivery efficiency and the short-term consequences on cell viability. When the delivery of gold nanorods was successful, we analyzed their mobility by mean squared displacement analysis. We found three populations of nanorods: immobile, freely diffusing and diffusing within a confinement. In zebrafish embryos cells all the mobile rods were freely diffusing, in HeLa cells the diffusing rods were about half and in COS1 cells about 70% of the total. The diffusion coefficients were around 0.006 $\mu m^2/s$, and the confinement radius was around 0.7 μm. By specific functionalization of gold nanorods with selected proteins, high-precision single-particle tracking of these particles can in the future be used to follow the dynamics of proteins in live cells in 3D with nm accuracy.

Single-Particle Tracking of Gold Nanorods in Live Cells, S.Carozza, V. Keizer, A. Boyle, A. Kros, M. Schaaf, J. van Noort. (in preparation).

3.1 Introduction

Single-molecule imaging has become an important technique for resolving the spatial and temporal distribution of molecules in cells. The choice of a suitable label is extremely important for single-molecule imaging *in vivo*: the brightness of the label determines the localization accuracy of the molecule of interest, and its stability in time limits the duration of the experiment. The signal of fluorescent proteins is typically rather weak for detection with high precision in a noisy environment like a living cell, and they exhibit low photostability due to bleaching or blinking. Organic dyes generally have better photophysical properties, but are still limited in their use.

The advantages of using gold nanoparticles (GNPs) as labels *in vivo* are many. The luminescence of GNPs is higher than the fluorescence of organic dyes, and does not suffer from bleaching or blinking. Among GNPs, gold nanorods (GNRs) can be excited in the IR region of light, where absorption by cells, and consequently photodamage, are minimized. The properties and advantages of GNRs are discussed in more detail in Chapter 1, Section 1.3.

The use of gold nanoparticles for applications in live cells was reported in many publications. Some focused on the mechanisms of uptake and localization of the particles inside cells (for a detailed review on the cell uptake of GNPs see [1]). In some cases, nuclear targeting of GNPs was achieved using nuclear localization signal (NLS) [2–4]. The efficiency of GNPs to generate highly localized heat when excited, joined to their easy functionalizability, makes them a preferred tool for thermal cancer therapy [5]. The uptake of GNRs in HeLa cells was studied by Ding [6] and Oyelere [7], who also functionalized GNRs with NLS for nuclear targeting. Huang and Durr [8, 9] used GNRs to specifically detect cancer cells. To our knowledge, a quantification of the dynamics of GNRs in live cells by single-particle tracking was performed only by Van den Broek [10]. As GNRs are very promising tools to study the dynamic of proteins *in vivo*, we believe that a more detailed study of their mobility inside cells is of high interest.

When passive delivery methods are used, nanoparticles enter the cell by endocytosis, and they remain trapped in vesicles [1, 11]. We used multiple alternative delivery methods to test whether GNRs can be introduced in cells without the internalization into vesicles, and whether

the choice of the delivery method has an influence on the mobility of the GNRs. Based on the images of cells taken shortly after the delivery, we evaluated the delivery efficiency and the impact of each method on the cells health.

Imaging was performed with a two-photon multifocal scanning microscope, which offers wide-field illumination and high localization accuracy in 3D. Trajectories of individual GNRs in the cells were obtained and further analyzed to quantify their mobility. We first inspected the MSD histograms of all traces and identified populations that exhibited different types of mobility. Then we performed a mean squared displacement analysis on single traces, to quantify mobility parameters. The difference in the mobility obtained for GNRs delivered with different methods is presented and discussed.

3.2 Materials and methods

Gold nanorods preparation

GNRs with a size of approximately 40 nm x 10 nm were prepared by seed-mediated synthesis [12]. Bifunctional α-mercapto-ω-amino Polyethyleneglycol-5000 (PEG-5000) was then added in excess to the GNRs solution, resulting in complete coverage of the GNRs surface with a PEG layer. PEGylation of GNRs is used to reduce cytoxicity in cells [13]. The solution was left to stir at room temperature overnight before the GNRs were centrifuged, the supernatant removed and the GNRs resuspended in phosphate buffered saline (PBS).

Cell culture

We tested two types of mammalian cells: HeLa and COS1. Cells were cultured in Dulbecco's modified eagle's medium (DMEM, Gibco) supplemented with 10% fetal calf serum (FCS) and were kept at 37 °C and 5% CO_2.

Delivery of gold nanorods in cells

Incubation of GNRs with mammalian cells
Incubation is the simplest technique to deliver particles into cells. A solution containing particles is added to the medium and cells are left in incubation, as depicted in Fig. 3.1a. The plasma membrane is impermeable for small solutes, while larger particles or particles with a high surface charge can be taken up by cells via endocytosis. The cells were trypsinized to detach them from the surface they adhered to. After trypsinization, a 30 nM GNR solution in PBS was added to the culture. After 5 minutes cells were placed in a well plate containing a glass coverslip immersed under DMEM containing FCS, and incubated for at least one hour.

Electroporation into mammalian cells
Delivery through electroporation is obtained by placing a cuvette containing cells and particles between two electrodes. Upon application of a voltage difference, the membrane forms temporary nanometer size pores due to local fluctuations in the transmembrane voltage. Small particles diffusing in the cuvette can thus enter the cells. The procedure is depicted in Fig. 3.1b. When fibronectin coated coverslips were used, 250 µl 10 µg/ml fibronectin in PBS was placed on coverslips and incubated for one hour at 37 °C. Subsequently, coverslips were washed once with an excess of PBS. HeLa or COS-1 cells were trypsinized, spun down and resuspended in 100 µl nucleofector solution (Lonza) and placed into cuvettes containing 3 nM of GNR solution. Next, cells were electroporated using the nucleofector II device (Lonza). Cells were spun down and resuspended in 800 µl DMEM containing 10% FCS. Cells were subsequentely plated onto coverslips and left to adhere at least 30 minutes prior to imaging.

Squeezing of GNRs into mammalian cells
This method involves pushing cells contained in a tube trough a small microfluidic channel by applying pressure on one side of the tube [14]. Due to the shearing stress that the cells experience in the narrow channel, gaps are created in the plasma membrane. Particles can then enter the cells via diffusion through these gaps. A scheme of the squeezing method is depicted in Fig. 3.1c. Before the experiment, cells were trypsinized, spun down, washed and suspended in 100 µl PBS. Freshly prepared 15

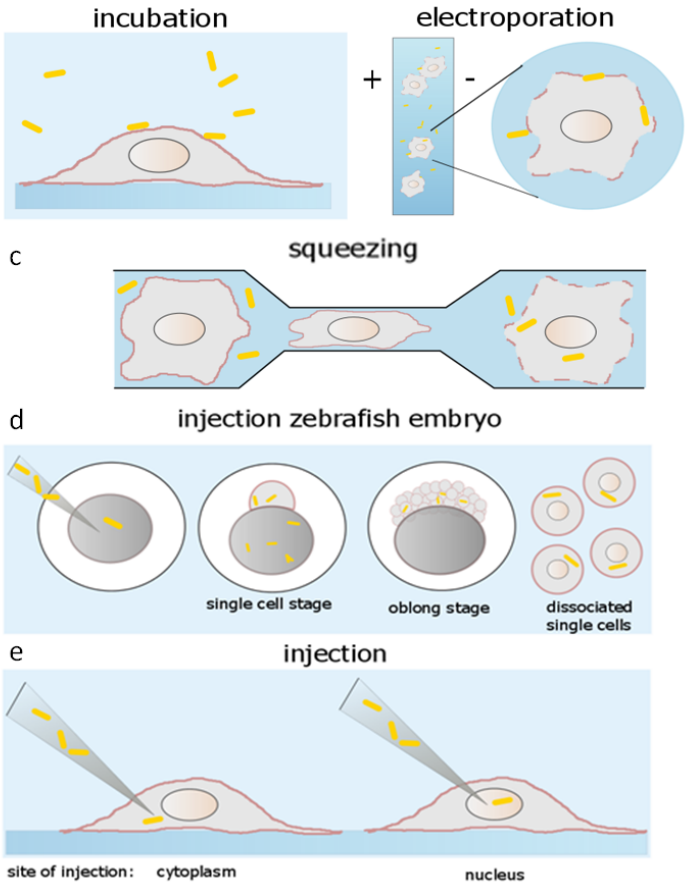

Figure 3.1
Schematic illustration of the methods used to deliver GNRs in cells. a) Incubation with cells, b) electroporation into cells, c) cell-squeezing, d) injection in the yolk of zebrafish embryos cells, e) microinjection in single cells. Drawing are not to scale.

nM GNR solution was added and the solution was flowed through the squeezing device (SQZ Biotech), using a pressure of 344 kPa. After 1.5 minutes 100 µl DMEM containing 10% FCS was added.

Injection of GNRs into zebrafish embryos
The yolk of a zebrafish embryo egg is surrounded by a chorion that can be easily visualized under a microscope and penetrated using a mi-

cropipette loaded with nanoparticles solution. When the egg is fertilized, a cell develops on top of the chorion. After multiple rounds of cell division, over a thousand cells result that take up the particles that were injected into the yolk. Fig. 3.1d depicts the injection procedure. Zebrafish were raised, grown and kept at 28.5 °C. Embryos were harvested and kept in egg water (Instant Ocean sea salts). Manually pulled micropipettes were loaded with 5 µl 0.3 nM GNRs. Injections were carried out at the single cell stage according to the protocol reported in [15]. The injected volume was equal to approximately one third of the yolk sac volume. Following injection, embryos were left to develop until the oblong stage at 28 °C. Embryos were then dechorionated using 1 mg/mL pronase (Sigma Aldrich) on a rotating stage for 30 seconds. Subsequent pipetting of the embroys resulted in dechorionation of the embryos. To dissociate the zebrafish cells, the embryos were incubated with 1 ml of calcium/magnesium free solution for 30 seconds. Cells were spun down and resuspended in 500 µl PBS. Zebrafish embryos cells were allowed to set for at least 30 minutes prior to imaging.

Injection of GNRs into mammalian cells
Fig. 3.1e depicts the direct injection of GNRs in single cells using micropipettes to penetrate the plasma membrane of individual cells. Either the cytoplasm or the nucleus of each individual adhering cell can be injected separately. One day prior to injection, cell samples were placed onto coverslips and covered with 1 ml of DMEM. Using a diamond pen two lines, crossing at a 30°angle, were scratched into the bottom of the coverslip to make a reference marker. Subsequently, the sample was placed under an inverted microscope using a 20x objective (Olympus). This microscope contained an additional support beam holding an injection arm (Eppendorf). A femtoject II needle (Eppendorf) was loaded with 3 µl 0.12 nM GNR solution in PBS using a microloader tip (Eppendorf). The micropipette was placed in the holder of the injection arm and connected to a femtojet pump (Eppendorf). A constant pressure of 150-250 hPa was supplied inducing a constant flow of GNR solution. Once the tip of the micropipette and cells were focused in the same plane, approximately ten cells were injected without interruption. Cells were incubated at 37 °C and 5% CO_2 for 30 minutes prior to imaging.

Imaging and tracking

We used a home-made two-photon multifocal scanning microscope for imaging. A pulsed IR laser (Chameleon Ultra, Coherent) was used for the excitation. A diffractive optical element (DOE, custom-made by Holoeye Photonics) divided the excitation beam in an array of 25x25 focal spots. The array was then scanned by a fast scanning mirror (FSM-300, Newport) to obtain a squared homogenous illumination. Using a piezo-actuator (P-726 Pifoc, PI) we moved the objective (60x APOTIRF, Nikon) in the z direction to acquire 3D images of the sample. Thanks to the wide-field illumination in 3D, we could image GNRs within the entire volume of one or more cells. A white-light LED placed above the sample was used for transmission images of the cells. A more detailed description of the setup can be found in Chapter 1, Section 1.2.3.

To follow the GNRs and monitor cells at the same time, a stack of fluorescence images and one transmission image were collected for every time point. The image size was typically 400 x 400 pixels (about approximately 60 μm x 60 μm. 3D stacks were made of 15-18 2D images, taken 0.5 μm from each other and acquired with a frame rate of 8 Hz. Fluorescence images were acquired with excitation at 770 nm. Fig. 3.2a shows an example of transmission image. A two-photon luminescence image made by a projection of all slices in a 3D stack is shown in Fig. 3.2b. Fig. 3.2c is a z-y reconstruction of the 3D stack, built by interpolating the pixel intensities between the z slices. Typically we acquired movies that lasted 10 minutes. In every frame of the 3D movie we localized small volumes of interest (typically 10 x 10 pixels in x, y and 5 slices in z) around each bright peak corresponding to a GNR. Then, we performed a 3D Gaussian fit on each volume of interest to obtain nanometer accurate 3D coordinates of the GNRs. Fig. 3.2d shows an example of the GNRs peaks, overlapped with the transmission image. The coordinates of a GNR in each time point were then connected into a trace, using a nearest-neighbor algorithm. In Fig. 3.2e the GNR traces are overlapped with the transmission image.

Mobility analysis

To quantify GNR mobility, we performed a mean squared displacement (MSD) analysis of the traces [16]. The MSD of a trajectory, as described

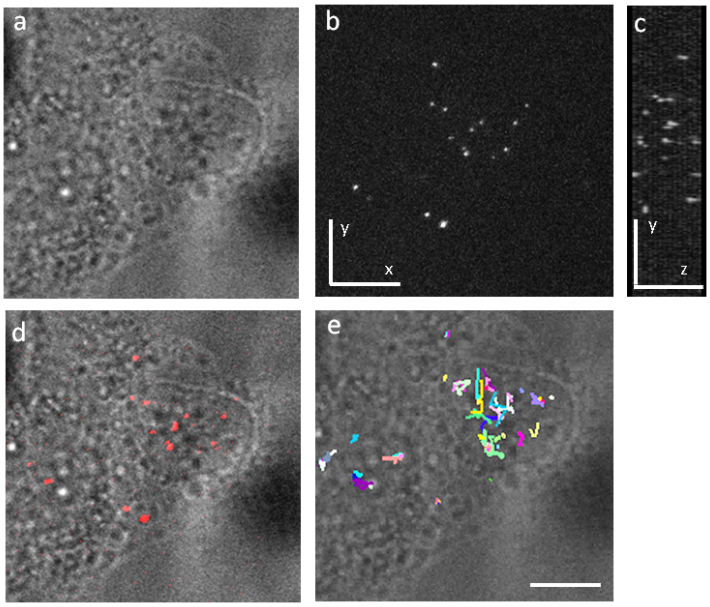

Figure 3.2
Image acquisition and traces reconstruction. a) An image of a HeLa cell microinjected with GNRs. A transmission image is collected for every 3D stack of fluorescence images. b) An example of a single frame in the 3D stack. c) A z-y image of the 3D stack. d) The overlap of a transmission image with the projection of all the two-photon luminescence frames in a stack. The two-photon signal is depicted in red. An overlap of the GNRs traces and the transmission image is shown in e), where each color represents a different trace. The scale bars correspond to 10 μm.

in Chapter 2, is defined as the average of the squared displacements covered by the particle in time steps of duration τ. The diffusion coefficient D is used to quantify the mobility of a particle. D depends on the size of the particle and on the temperature and viscosity of the medium, according to the Stokes-Einstein equation (Eq. 2.4 in Chapter 2).

If the particle is freely diffusing, the MSD is a linear function of τ with a slope that depends on the diffusion coefficient D:

$$MSD(\tau) = 6\sigma^2 + 6D\tau \tag{3.1}$$

and an offset that depends on the localization accuracy σ of the system. Fig. 3.3a shows an example of a freely diffusing GNR. Its MSD plot and

the fit with Eq. 3.1 are shown in Fig. 3.3b.

When the movement of the particle is directional (superdiffusion), a quadratic component, dependent on the velocity v, introduces a positive curvature in the MSD:

$$MSD(\tau) = 6\sigma^2 + 6D\tau + v^2\tau^2 \tag{3.2}$$

If the diffusion of the particle is confined (subdiffusion or confined diffusion) the MSD exhibits a negative curvature. The shape of MSD for a trace confined within a spherical area approximates to [17]:

$$MSD(\tau) = 6\sigma^2 + \frac{6R^2}{5} - 12R^2 \sum_{n=1}^{\infty} exp\Big[-\beta_{1n}^2 \frac{Dt}{R^2}\Big] \frac{1}{-\beta_{1n}^2(-\beta_{1n}^2 - 1)} \tag{3.3}$$

where R is the confinement size and β_{1n} are constants given by the solutions of the spherical Bessel function of the first order. An example of a confined trace and its MSD are shown in Fig. 3.3c,d.

The localization accuracy of the system and the number of points in a trajectory determine the precision of its MSD and thus the precision of D (as explained in detail in Chapter 2, Section 2.3.2, [18]). The error on each MSD point is strongly influenced by the length of the trajectory: the MSD points have increasing uncertainties, due to the decreasing number of steps used to calculate the mean (see Eq. 2.3 in Chapter 2). The presence of a curvature in the MSD plot can therefore be hidden in the standard deviation of the MSD points. For this reason, choosing the mobility model based on single traces is not reliable when dealing with large fluctuations in MSD due to short trajectories. Alternatively, we analyzed the distribution of the MSD of all traces at different time steps to identify populations following different models. Based on changes in the ensemble distributions, a threshold was set to divide different modes of mobility. MSD analysis was subsequently performed on individual traces to quantify the mobility parameters of single GNRs. This approach allows for distinguishing free from confined populations, but unfortunately not from active populations.

Traces shorter than 4 time points (about 8 s) were excluded from the analysis. To identify immobile GNRs we used a threshold based on the localization accuracy of the setup, calculated as explained in Chapter 2 (Eq. 2.1). The localization accuracy is inversely proportional to the square root of the photon emission intensity of the GNRs (Fig. S1).

Typically, the localization accuracy in 3D was about 40 nm. GNRs showing a MSD at any time delay lower than the square of the localization accuracy, multiplied by 6 (i.e. 0.0096 μm^2) were considered immobile. An example of immobile trace, its MSD and fit are plotted in Fig. 3.3e,f.

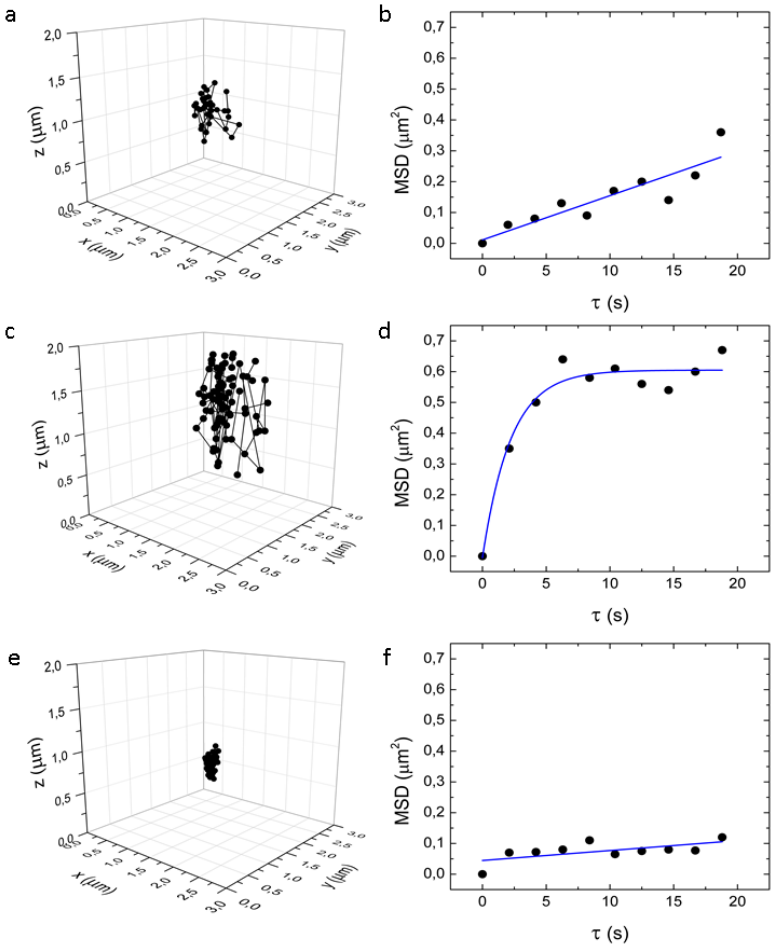

Figure 3.3
Examples of time traces of single GNRs showing 3 different modes of movement, along with the corresponding MSD plot. a) Trace of a freely diffusing GNR and b) its MSD plot fitted to Eq. 3.1. c) Trace of a GNR featuring confined diffusion and d) its MSD fitted to Eq, 3.3. e) Trace of an immobile GNR and f) its MSD plot fitted to Eq. 3.1.

The MSD analysis of GNRs traces was performed in LabVIEW. To

assess the significance of differences in the mobility of GNRs from different samples, we used a Single-Factor Analysis of Variance (ANOVA), with a p-value threshold of 0.05. For non-normal distributions, the Kruskal-Wallis ANOVA test was used.

3.3 Results

3.3.1 Delivery in cells and considerations on cell viability

Fig. 3.4 shows some examples of HeLa cells after delivery of GNRs with different methods. The delivery through incubation in a solution containing GNRs was not successful: GNRs resided in the medium or were stuck around the external membrane (Fig. 3.4a, b). The round shape of the cells is due to the trypsinization process that disrupted the proteins involved in the adherence of the cell to the coverslip. HeLa cells containing GNRs delivered through electroporation are shown in Fig. 3.4c, d. In some cases, the coverslip was functionalized with fibronectin, to facilitate the cell adherence, but we did not observe any difference in cells spreading. The delivery was successful, but not all the cells looked healthy. The cells were imaged about 1 hour after electroporation. Fig. 3.4e, f shows two cells after undergoing cell-squeezing with GNRs. The delivery was not successful: we observed only GNRs outside cells or stuck around the external membrane. All the cells showed very poor conditions after the procedure: a large fraction died, while many of the survivors could not adhere properly to the glass. The images were taken about 1 hour after the squeezing procedure. Two images of HeLa cells microinjected with GNRs in the nucleus (Fig. 3.4g) and in the cytoplasm (Fig. 3.4h) are shown. The delivery was successful and most of the cells appeared in good condition, as judged by their shape. Cells were imaged about half an hour after the injection.

We also tested some of the delivery techniques in COS1 cells. Examples of the results are shown in Fig. 3.5. Incubation (Fig. 3.5a, b) was not successful, as in the case of HeLa cells. Also in the case of COS1 cells, the round shape is due to the trypsinization process. The delivery of GNRs through squeezing (Fig. 3.5c, d) was successful only in few cases. Similarly to HeLa cells, squeezed COS1 cells showed very poor conditions.

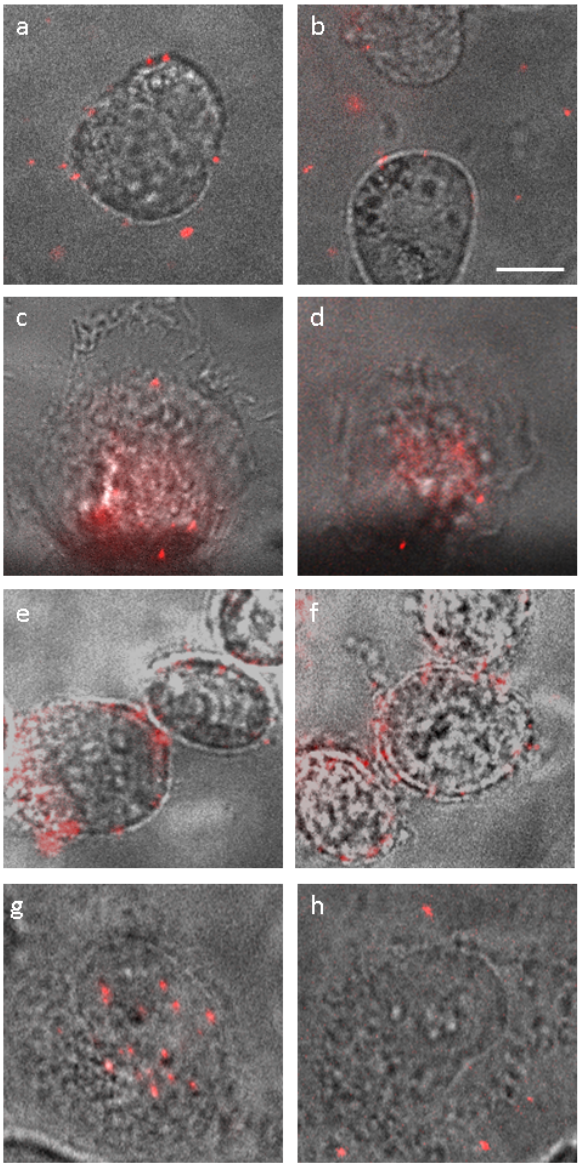

Figure 3.4
Images of HeLa cells after GNR delivery using different techniques. a,b) Two examples of cells incubated with GNRs after trypsinization. c, d) Two cells electroporated with GNRs. e,f) Two images of cells squeezed with GNRs. Two images of HeLa cells, microinjected g) in the nucleus and h) in the cytoplasm. Red marks indicate the two-photon luminescence signal of GNRs. The scale bar corresponds to 10 μm.

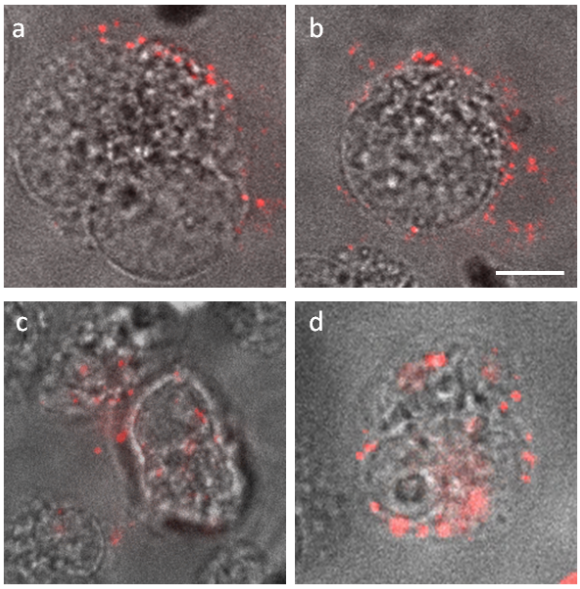

Figure 3.5
Images of COS1 cells after GNR delivery via different techniques. a,b) Two COS1 cells incubated in a solution containing GNRs after trypsinization. c,d) Two COS1 cells squeezed with GNRs. The scale bar corresponds to 10 μm.

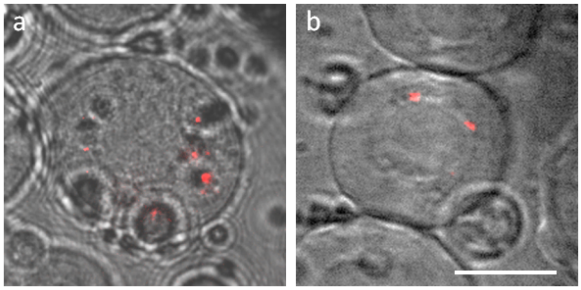

Figure 3.6
Zebrafish embryos cells after delivery of GNRs through injection in the egg yolk. The scale bar corresponds to 10 μm.

Fig. 3.6 shows two zebrafish embryos cells after injection in the embryo yolk. The delivery efficiency was high and cells were in good conditions. Imaging was performed 6 hours after injection.

In conclusion, successful delivery was observed using electroporation and single-cell microinjection in HeLa cells, squeezing in COS1 cells and injection in the yolk of zebrafish embryos cells, though differences in cell viability were observed.

3.3.2 Mobility of gold nanorods in cells

We next analyzed the mobility of GNRs microinjected in the cytoplasm and in the nucleus of HeLa cells, delivered through electroporation in HeLa cells, through cell-squeezing in COS1 cells and injected into zebrafish embryos cells. In none of the cells we observed translocation of GNRs from the cytoplasm to the nucleus in the duration of the experiment (up to 3 hours after delivery).

In most of the cases, the GNRs traces were shorter than 1 minute (Fig. S1). A short trajectory results in relatively large errors in the MSD points. Thus, we could not reliably choose a model to fit the trace based on the slope of the MSD curve. Instead, we plotted the distributions of the MSD at different delays. Fig. 3.7 shows the histograms of the MSD for each GNR sample, for each time step, normalized for the total number of traces in the distribution. Next, we divided the traces in populations following different models by a visual inspection and thresholding of the MSD histograms in time.

The MSD histograms representing GNRs microinjected in cytoplasm are shown in Fig. 3.7a. We observed the presence of a stable population with MSD below 0.2 μm^2 in all four time points, probably due to the presence of a confinement. Note that these MSDs all exceed the threshold for immobilization. MSD values higher than 0.1 μm^2 for $\tau = 6.5$ s, typically increased over time, a sign of free diffusion. We tested whether this mobile fraction is compatible with a population with a single diffusion coefficient D. From the center of the distribution at the last time point ($\tau = 6.4$ s), we estimated D to be around 0.01 $\mu m^2/s$. The width of the MSD expected for traces with a typical length of 20 points and a diffusion coefficient of 0.01 $\mu m^2/s$ is however significantly smaller (Fig. S2) than the distribution shown in Fig. 3.7a.

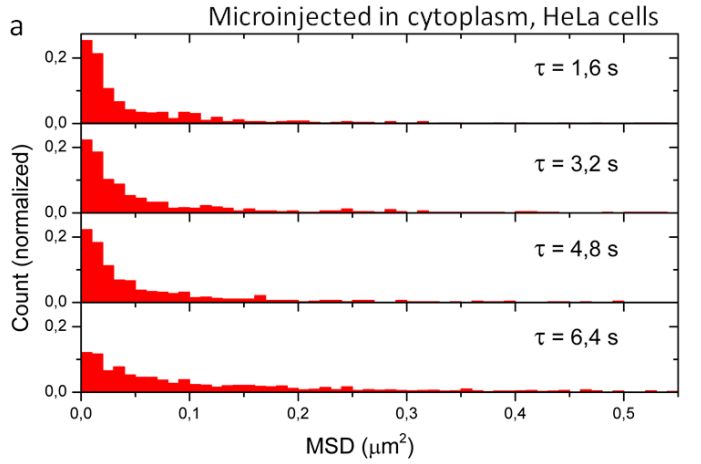
a
Microinjected in cytoplasm, HeLa cells
τ = 1,6 s
τ = 3,2 s
τ = 4,8 s
τ = 6,4 s
Count (normalized)
MSD (μm²)

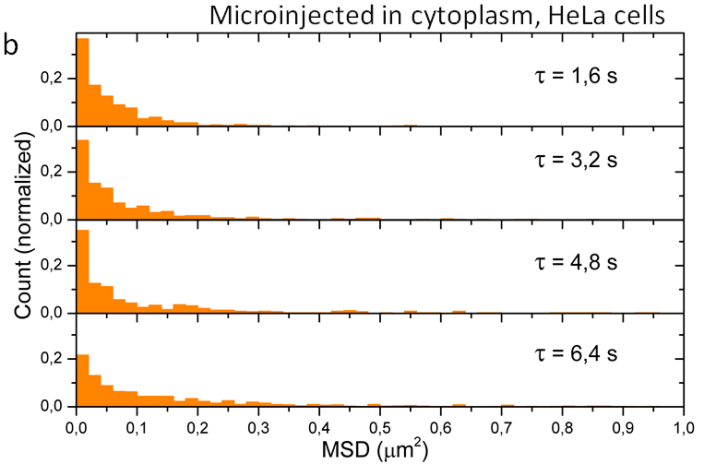
b
Microinjected in cytoplasm, HeLa cells
τ = 1,6 s
τ = 3,2 s
τ = 4,8 s
τ = 6,4 s
Count (normalized)
MSD (μm²)

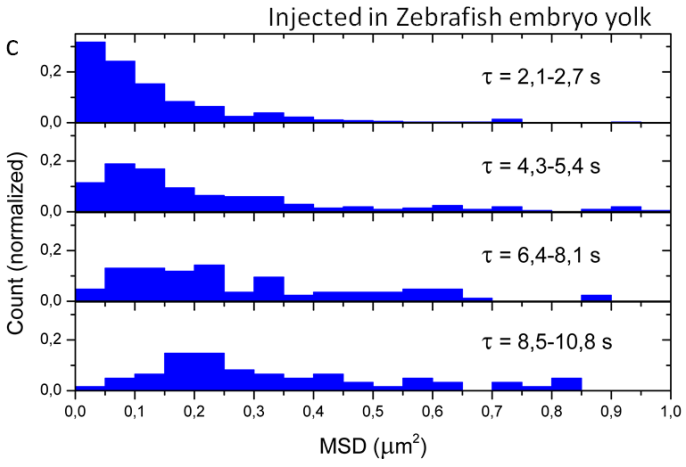
c
Injected in Zebrafish embryo yolk
τ = 2,1-2,7 s
τ = 4,3-5,4 s
τ = 6,4-8,1 s
τ = 8,5-10,8 s
Count (normalized)
MSD (μm²)

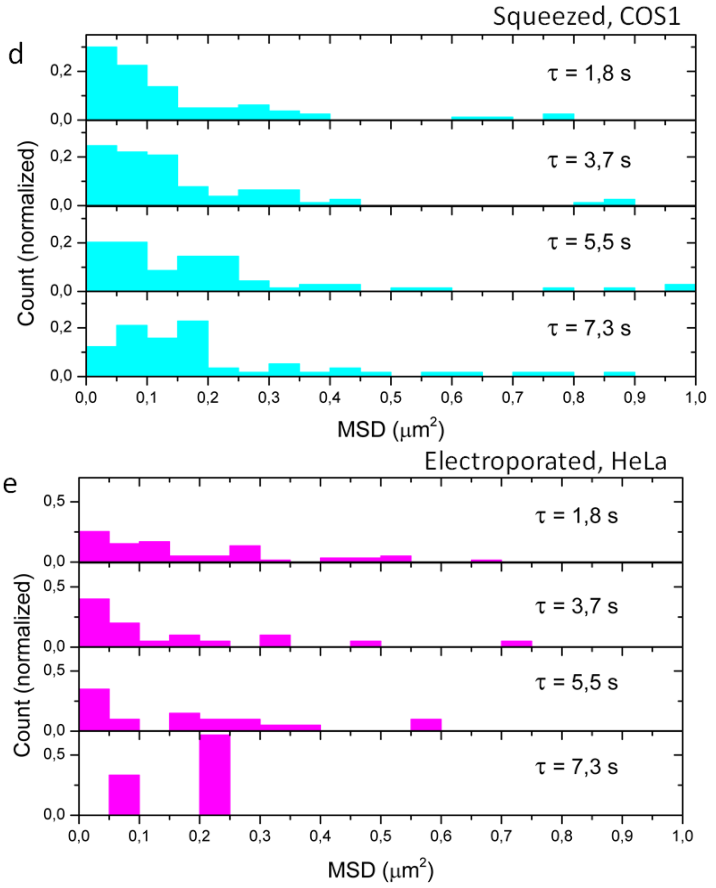

Figure 3.7
Histograms of MSD divided by time step. MSD histograms from traces of GNRs a) microinjected in cytoplasm of HeLa cells, b) microinjected in nucleus of HeLa cells, c) microinjected in zebrafish embryos cells, d) in squeezed COS1 cells and e) in electroporated HeLa cells. A small fraction, typically $< 5\%$, exceeding MSD $= 1$ μm^2, is not shown. We attribute such fraction to artifacts originating from erroneous connection of peaks.

This result points to a variety of diffusion constants in this population that can be only be revealed by single-particle analysis.

Using a MSD threshold of 0.1 μm^2, we distinguished between two populations. The first one appears to have a constant MSD, consistent with confined diffusion. The second population shows a growth of MSD with increasing time lags, indicative of free diffusion. We divided the traces into these two categories by setting a threshold of their MSD at 6.4 s. We fitted the MSD of individual traces belonging to the first population with Eq. 3.3, and we used Eq. 3.1 for the MSD of traces of the second population.

The MSD histograms of the GNRs injected in nucleus of HeLa cells (Fig. 3.7b) are very similar to the histogram of GNRs in cytoplasm. Therefore the two samples were analyzed in the same manner.

The MSD histograms of GNRs injected in zebrafish embryos cells reveal a different behavior (Fig. 3.7c). As opposed to GNRs in HeLa cells, we did not observe a population with MSD independent of the time lag: therefore we analyzed all traces with the free diffusion model. In this case, movies with different frame rates were acquired, resulting in multiple MSD series. To increase the sample size, we aggregated the MSD into single histograms.

In squeezed cells both a stable and a mobile population were found in the MSD histograms (Fig. 3.7d). The statistic was quite small as compared to microinjected GNRs. Because it is harder to draw a threshold between the two populations, we used the same threshold as used for the HeLa cells at 0.1 μm^2. A time lag of 7.3 s was used to distinguish the two populations.

The MSD histograms of GNRs in electroporated cells are shown in Fig. 3.7e. The size of this sample is small, but nevertheless we can see a stable population at low MSD values. Note that the histogram at the fourth time point is built from only three traces; we considered these peaks to be outliers due to large fluctuations. We used again a threshold of MSD = 0.1 μm^2 at $\tau = 5.5$ s and distinguished two populations.

After dividing the populations in each sample, we analyzed the single traces with the corresponding diffusion (Eq. 3.1) or subdiffusing model (Eq. 3.3). We obtained a distribution of the diffusion coefficients and of the confinement sizes as shown in Fig. 3.8. The independence of the MSD of time lag of the confined population suggests that the particles reached the confinement within the first step: therefore we expected not to be able to fit the diffusion coefficient correctly in these traces, but only the confinement size. Given a confinement radius of 0.2-0.6 μm, we

estimate the diffusion coefficient of confined GNRs to be around 0.02-0.06 $\mu m^2/s$. Note that the MSD is larger than the expected positional accuracy, so these confined GNRs are indeed mobile.

The mobility parameters obtained are summarized in Table S1. In the table we reported the number of traces for each mode and the relative percentage on the total population, the median, the 1st and the 3rd quartiles of the parameter distribution. In both injected and electroporated HeLa cells, we found a fraction of immobile GNRs equal to about 15%. This fraction is almost absent in squeezed COS1 cells (1%), and it is higher in zebrafish embryos cells (30%). The freely diffusing population amounts to 42% of the traces in the case of GNRs microinjected in cytoplasm and 49% of the GNRs microinjected in nucleus, 57% of the GNRs in electroporated cells and 76% of the GNRs in squeezed cells. In zebrafish embryos cells we did not observe confined diffusion: all mobile rods (71%) appear to be freely diffusing.

Population	Parameter	Injection HeLa Cytoplasm	Injection HeLa Nucleus	Injection ZF embryos yolk	Squeezing COS1	Electrop. HeLa
Immobile	Pop. Size	125; 13%	107; 16%	24; 30%	1; 1%	7; 15%
Confined	Pop. Size	449; 45%	225; 35%	0	14; 23%	13; 28%
	Confinement (μm)	0.2 (0.1-0.4)	0.3 (0.2-0.4)		0.3 (0.2-0.5)	0.4 (0.3-1)
Freely Diffusing	Pop. Size	418; 42%	316; 49%	59; 70%	47; 76%	26; 57%
	D ($\mu m^2/s$)	0.006 (0.003-0.009)	0.007 (0.004-0.01)	0.004 (0.003-0.006)	0.006 (0.004-0.01)	0.006 (0.004-0.01)

Table 3.1
Mobility parameters of GNRs delivered in cells with different methods. The number of traces used for the statistics, the percentage relative to the total number of traces, the median, 1^{st} and 3^{rd} quartiles of the diffusion coefficient and of the confinement sizes are reported for the free and confined population.

The distribution of diffusion coefficients (Fig. 3.8a) presents comparable characteristics for different delivery methods. In none of the cases

we observed a normal distribution: the histograms are shown in Fig. S3. The diffusion coefficients (Table S1) have median values between 0.004 and 0.007 $\mu m^2/s$. No significant difference between the diffusion coefficients was found using a non-parametric ANOVA (Kruskal-Wallis) test.

In squeezed COS1 cells and in both injected and electroporated HeLa cells, we found a fraction of GNRs with mobility that appears to be confined. This fraction consists of 55% of the GNRs in the cytoplasm and 46% in the nucleus of microinjected cells, 23% in squeezed cells and 35% in electroporated cells. The distributions of confinement sizes are shown in Fig. 3.8b. In all four distributions a wide range of confinement sizes was observed, from 70 nm (below this limit we define GNRs as stuck) to 10 μm. The median values are between 0.2 μm and 0.4 μm. Outliers with large confinement sizes are present in all the cases but are especially numerous among GNRs in cytoplasm and nucleus of microinjected HeLa cells. However, we measured a larger number of samples for those measurements. The confinement sizes in squeezed and electroporated cells are a bit larger than in microinjected HeLa cells, but there is no significant difference between the four populations. Histograms of the confinement sizes distributions are plotted in Fig. S4.

3.4 Discussion and conclusion

In this study, we tested different methods to deliver GNRs in live cells: incubation with HeLa and COS1 cells, electroporation into HeLa cells, cell-squeezing of Hela and COS1 cells, injection in zebrafish embryos cells and microinjection in single HeLa cells. We analyzed the mammalian cells shortly after delivery of GNRs, but had to wait a few hours in the case of zebrafish embryos cells to allow cell division. In the case of incubated cells we obtained a low number of GNRs. It is possible that not enough time was given to the GNRs to enter the cells [19]. Also for electroporated cells, waiting a longer time before imaging might increase the delivery efficiency [20], even though successful delivery has been reported few minutes after electroporation [21].

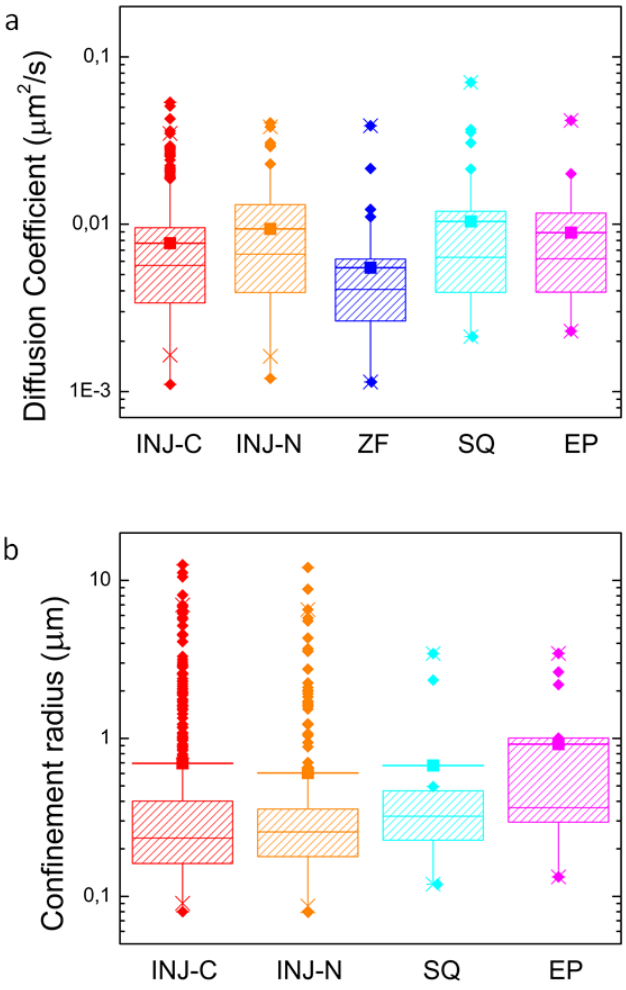

Figure 3.8
Distribution of mobility parameters for GNRs in cells. a) Distribution of diffusion coefficients of GNRs freely diffusing in cells and b) distribution of confinement sizes of GNRs undergoing confined diffusion in cells, split out by delivery technique. The box-plots are defined as follows: the box include data from the 25^{th} to the 75^{th} percentile; the vertical line goes up to the 90^{th} percentile. Outliers above the 90^{th} percentile are plotted. Crosses mark the 1^{st} and 99^{th} percentiles. The square on horizontal line indicates the average of the distribution, and the horizontal line without square indicates the median. Note that the sample sizes of microinjected cells in cytoplasm and nucleus (INJ-C and INJ-N) are much larger, explaining the larger number of outliers for these fractions.

Squeezed cells showed low delivery efficiency. Although cell-squeezing was reported to be successful with small particles [14], it was never performed using particles of a size comparable to our GNRs: it is possible that the pores created in the cell membrane by this method were not large enough. Nevertheless, we observed poor cell viability after squeezing that was not mentioned in previous reports [14, 22].

The delivery yield of injection in zebrafish embryos yolk and microinjection in single HeLa cells was good, as well as the cell viability. These methods appeared the most gentle for delivering GNRs in cells. However, each of them has a downside: in the case of injection in yolk the imaging cannot be performed till few hours after the delivery, while in case of single cell microinjection there is a limited throughput. An advantage of microinjection in single cell is the possibility to selectively deliver in the cytoplasm or in the nucleus.

When the delivery was successful, we localized GNRs inside cells and analyzed their trajectories to obtain mobility information. We recorded GNRs traces ranging from few seconds to 7 minutes long, even though the typical duration of our movies was of about 10 minutes. Most of the traces we obtained were shorter than 1 minute. It was not clear why GNRs disappeared (or appeared) during the movie. It is possible that the index of refraction around a GNR changed, due to non-specific interaction with molecules or to the diffusion inside an area with different characteristics. A change in the dielectric constant induces a shift in the plasmon resonance peak of the GNR (as explained in Chapter 1, Section 1.3.2). As a result, the GNR cannot be excited anymore at the same wavelength. A similar 'blinking' behavior of gold nanoparticles in cell was already observed, but not investigated in detail [19]. Alternatively, reshaping of GNRs could occur, inducing a blue-shift in the spectrum. The excitation intensity range we used (typically around 0.1 kW/cm^2) is several orders of magnitude lower than threshold for complete GNR melting *in vitro* [23]. However, it could be sufficiently high to start the reshaping proces of the nanorods. Several studies about GNRs reshaping have been reported, both in solution [24, 25] and at single nanorod level [26], that revealed a strong dependence of the reshaping threshold on the size and aspect ratio of the particles and on the excitation pulse width. In addition, the medium and the presence of a PEG layer around the GNRs can also influence the reshaping threshold, by changing the ther-

mal conductivity [27]. For future experiments it should be investigated whether GNRs reshaping occurs in the excitation energy range we use, also taking into consideration the non-linear nature of the two-photon process.

Due to the short trace length and consequently the large error on MSD points, we could not characterize the mobility of individual traces with sufficient detail to identify different modes of mobility. We instead distinguished different mobility characteristics from the ensemble MSD histograms, and then fitted the traces belonging to each population accordingly.

In microinjected and electroporated HeLa cells we found a fraction of immobile GNRs equal to about 15% of the total number of traces. In zebrafish embryos cells this fraction is larger (30%), whereas it is almost absent in squeezed cells (1%). These immobile GNRs could be attached to immobile structures in the cell, such as stuck vesicles. Squeezed cells showed very poor viability, and it may be that most of the cellular structures were destroyed, explaining the extremely low percentage of stuck GNRs. The fraction of immobile GNRs was twice as large in zebrafish embryos cells. The difference in the cellular structure between zebrafish embryos cells and mammalian cells could explain the difference in the immobile fraction. The immobility of GNRs cannot be explained by the presence of large GNR clusters that would diffuse slower: from the distribution of the GNRs intensities, we estimated a percentage of clusters of only about 3% (Fig. S1).

Two populations of mobile GNRs were found: a freely diffusing one and one diffusing within a confined space. The diffusing population was 42% of the total in the nucleus of microinjected HeLa cells, 49% in the cytoplasm, 57% in electroporated cells and 76% in squeezed cells. In zebrafish embryos cells all the mobile rods (71%) were freely diffusing. Note that the size of the diffusing fraction is calculated based on a manually set threshold, and therefore it must be interpreted as indicative. All the GNRs in zebrafish embryos cells were freely diffusing.

The expected diffusion coefficient of GNRs inside cells can be calculated from the size of the particles and the viscosity of the environment (Eq. 2.4 in Chapter 2). GNRs are covered with a layer of PEG that increases their size: we calculated the hydrodynamic radius of PEG using fluorescence correlation spectroscopy (FCS) measurements (see Chapter

2, S1). The hydrodynamic radius of the GNRs is approximately 24 nm, though variations can occur due to the size variability within the GNRs sample. The value of intracellular viscosity is more difficult to quantify: it was reported to be similar [28, 29] to up to 3.2 times higher than the viscosity of water [30]. A recent review on the chemistry of the cytoplasm [31] however, concludes that it is inaccurate to consider the cytoplasm as a homogeneous solution with a single viscosity value: areas with different viscosities are present, due to phase-separation phenomena induced by crowding. The viscosity inside the nucleus was reported to be the same as in the cytoplasm, as the two compartments are communicating [32]. Assuming an intracellular viscosity between 1 and 4 times the viscosity of water yields a diffusion coefficient between 2 and 10 $\mu m^2/s$, about three to four orders of magnitudes higher than the values we obtained, around 0.006 $\mu m^2/s$ in all cases. Our results are compatible with the diffusion coefficients obtained previously in our group [10]. To explain such low values, we hypothesized at the time that GNRs were internalized into vesicles, in agreement with other authors that claim that nanoparticles can hardly escape internalization into vesicles [1]. This was also the motivation to explore alternative delivery methods that do not depend on endocytosis. However, the diffusion coefficients that we obtained here are surprisingly similar both in the cytoplasm and in the nucleus. As a vesicles system is not present in the nucleus, this claim cannot hold. The GNRs diffusion could be slowed down by the high crowding present in the nucleus, resulting in a value similar to the diffusion of vesicles in the cytoplasm. Another hypothesis is that the calculation of the diffusion coefficient should consider the presence of obstacles and temporary stickiness of the GNRs, which would effectively slow down the GNRs. However this would require detailed knowledge of the precise structure in each cell.

In HeLa and COS1 cells we found a population of GNRs with a MSD independent of the time lag, compatible for example with the enclosure by structural elements within the cellular environment. From the MSD analysis of this GNR population we obtained a wide range of confinement radii, from about 100 nm to 1 μm. These values are compatible with the range of sizes of compartments in cells: from vesicles of few hundreds of nm [33], to accessible spaces in the nucleus or between the plasma membrane and the nuclear membrane. Some outliers are present in the distribution (less than 10%), going from 1 μm up to 10 μm. As our

traces are too short for the GNRs to be able to encounter such large confinements, we therefore hypothesize that these confinement radii are the result of the large stochastic variations of the MSD for short traces. On the other hand, some freely diffusing GNRs can have a MSD lower than the threshold we set for confined particles, but they cannot be distinguished a priori.

The absence of a confined population in zebrafish cells can be due to a lower density of cellular structures as compared to mammalian cells. This could also suggest that injection in yolk is an effective way to escape the GNRs internalization into organelles.

Overall, we found a large similarity in the mobility of GNRs in HeLa and COS1 cells with a relatively large fraction of confined GNRs. The diffusion coefficient of GNRs in zebrafish embryos cells was a bit lower than in HeLa and COS1 cells, yet in the same order of magnitude. The values we obtained are lower than the D expected for particles of the same size moving inside cells, but the calculation of the expected D does not take into account stickiness, obstacles nor variations in viscosity.

The precision of our analysis could be improved by acquiring longer GNRs trajectories that would reduce the error on the MSD points. In this way, a reliable attribution to a mobility model could be carried out for every single trajectory, making possible also to distinguish superdiffusive from diffusive traces. Including an analysis of the direction of the movement [34], which also becomes more reliable for longer traces, can further help to quantify the deviation from purely diffusive motion. Longer traces can be achieved by increasing the frame rate of the microscope, or by extending the duration of the GNR signal. More investigation must be carried on the apparent blinking/bleaching behavior of GNRs that we observe in cell.

As next step, we will verify the functionalization of GNRs in order to target specific structures or proteins in the cell. High precision and long-time single-particle tracking of GNRs has a great potential for the study cellular processes in live cells.

3.5 Supplementary figures

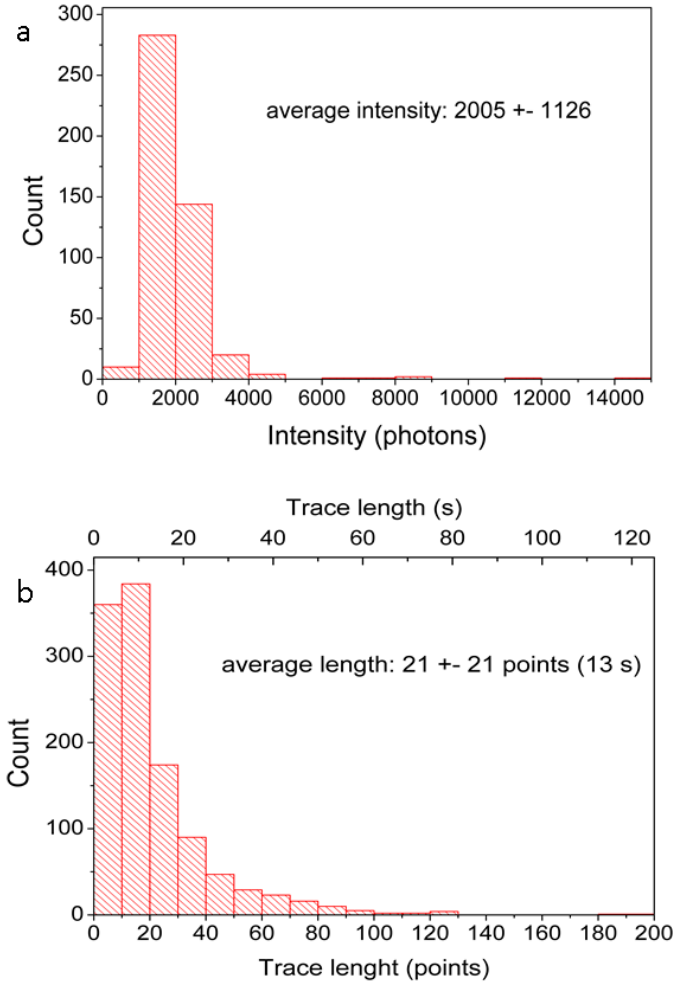

Figure S1
Distribution of a) intensities and b) trace lengths of GNRs microinjected in cytoplasm of HeLa cells.

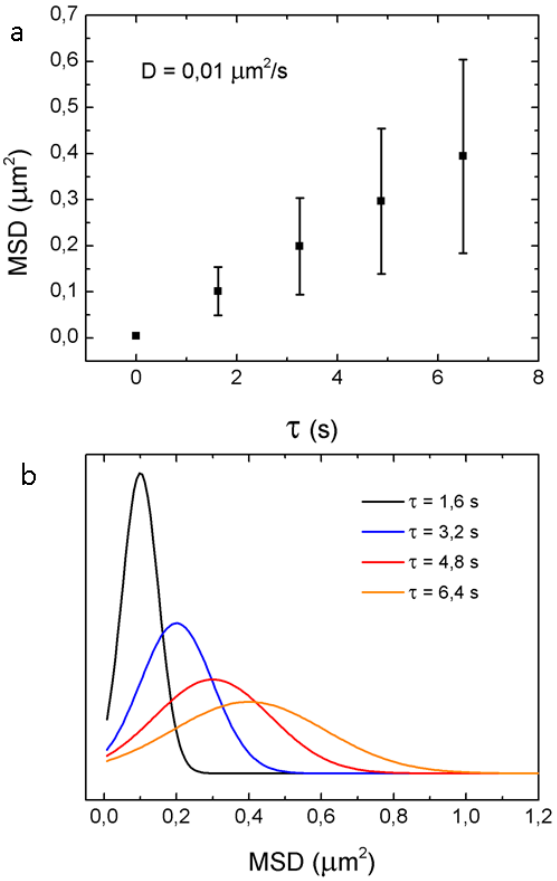

Figure S2
Simulated MSD of a particle moving with $D = 0{,}01\ \mu m^2/s$ in a trace of 20 points. a) MSD plot vs time step τ. b) Simulation of the distributions of the MSD populations at each time step τ.

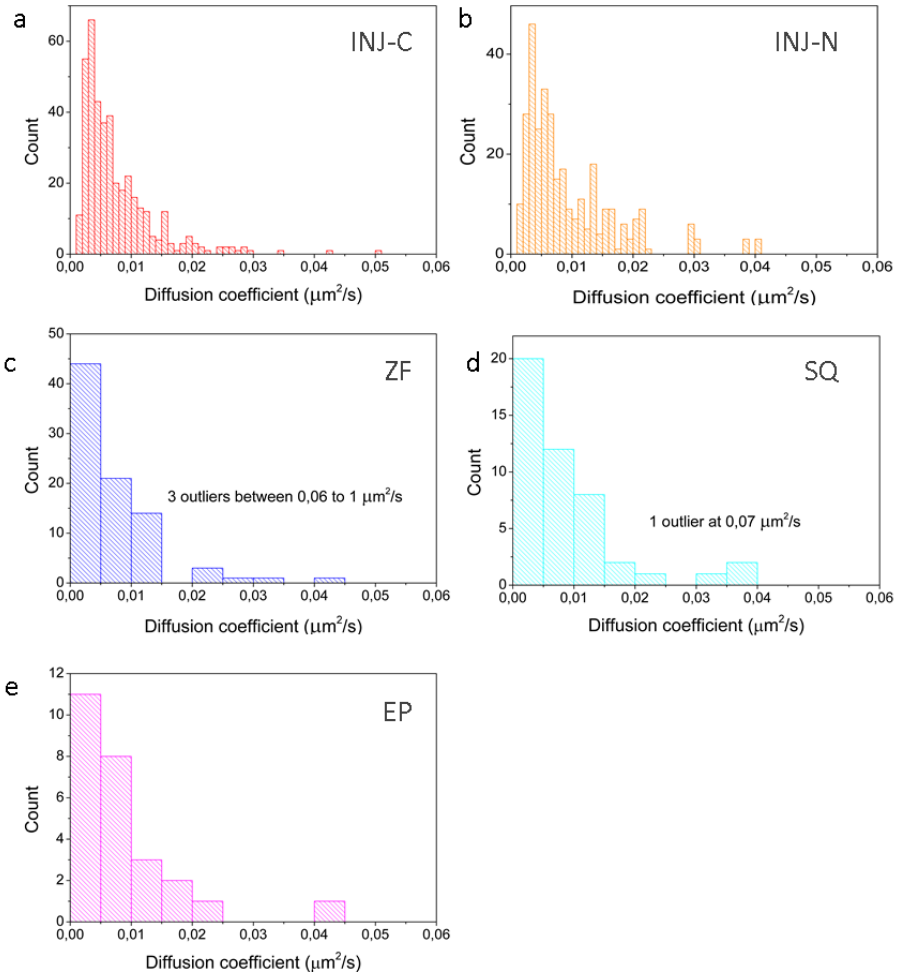

Figure S3

Histograms of distributions of the diffusion coefficients for GNRs microinjected in a) cytoplasm and b) nucleus of HeLa cells, c) injected in the yolk of zebrafish embryos cells, d) delivered in squeezed cells and e) in electroporated cells. The bin size is changed between experiments depending on the sample size: 0,001 in a,b and 0,005 in c,d,e.

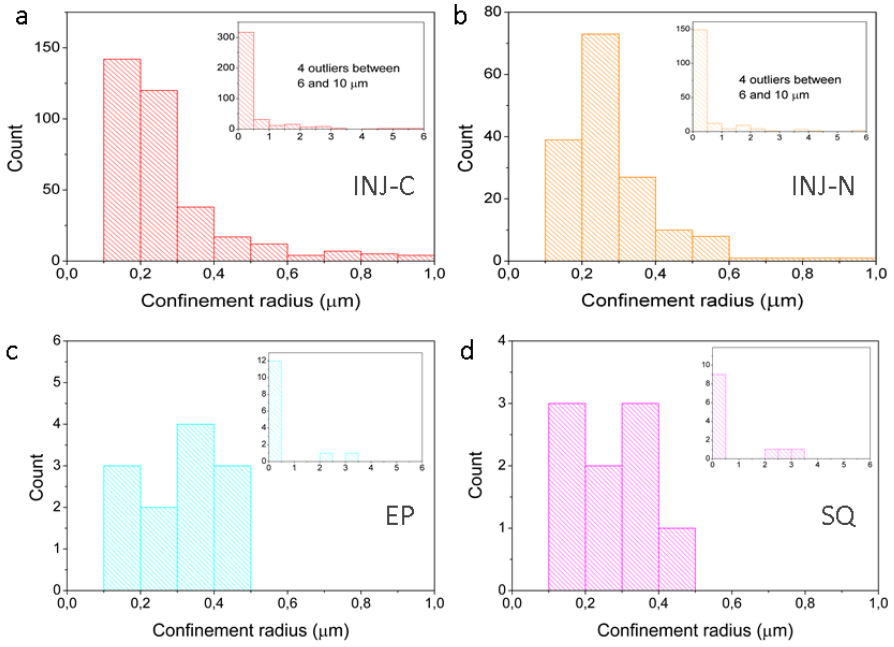

Figure S4

Histograms of distributions of the confinement radii for GNRs a) microinjected in the cytoplasm or b) microinjected in the nucleus of HeLa cells, c) in squeezed cells or d) in electroporated cells, in the range between 0 and 1 μm. Insets show zoom-outs of the histograms.

Bibliography

[1] Raphaël Lévy et al. "Gold nanoparticles delivery in mammalian live cells: a critical review." In: *Nano reviews* 1 (Jan. 2010). ISSN: 2000-5121.

[2] Wei Qian et al. "Dark-field light scattering imaging of living cancer cell component from birth through division using bioconjugated gold nanoprobes". In: *Journal of Biomedical Optics* 15.4 (2010), p. 046025. ISSN: 10833668.

[3] Paola Nativo, Ian Prior, and Mathias Brust. "Uptake and intracellular fate of surface-modified gold nanoparticles." In: *ACS nano* 2.8 (Aug. 2008), pp. 1639–44. ISSN: 1936-086X.

[4] Cécile Leduc et al. "Single-molecule imaging in live cell using gold nanoparticles." In: *Methods in cell biology* 125 (Jan. 2015), pp. 13–27. ISSN: 0091-679X.

[5] Nardine S. Abadeer and Catherine J. Murphy. "Recent Progress in Cancer Thermal Therapy Using Gold Nanoparticles". In: *The Journal of Physical Chemistry C* 120.9 (Mar. 2016), pp. 4691–4716. ISSN: 1932-7447.

[6] Hong Ding et al. "Gold Nanorods Coated with Multilayer Polyelectrolyte as Contrast Agents for Multimodal Imaging". In: *The Journal of Physical Chemistry C* 111.34 (Aug. 2007), pp. 12552–12557. ISSN: 1932-7447.

[7] Adegboyega K. Oyelere et al. "Peptide-conjugated gold nanorods for nuclear targeting." In: *Bioconjugate chemistry* 18.5 (2006), pp. 1490–7. ISSN: 1043-1802.

[8] Xiaohua Huang et al. "Cancer cell imaging and photothermal therapy in the near-infrared region by using gold nanorods." In: *Journal of the American Chemical Society* 128.6 (Feb. 2006), pp. 2115–20. ISSN: 0002-7863.

[9] Nicholas J Durr et al. “Two-photon luminescence imaging of cancer cells using molecularly targeted gold nanorods.” In: *Nano letters* 7.4 (Apr. 2007), pp. 941–5. ISSN: 1530-6984.

[10] Bram van den Broek et al. “Parallel nanometric 3D tracking of intracellular gold nanorods using multifocal two-photon microscopy.” In: *Nano letters* 13.3 (Mar. 2013), pp. 980–6. ISSN: 1530-6992.

[11] Peter Sandin et al. “High-Speed Imaging of Rab Family Small GTPases Reveals Rare Events in Nanoparticle Trafficking in Living Cells”. In: *ACS Nano* 6.2 (Feb. 2012), pp. 1513–1521. ISSN: 1936-0851.

[12] Babak Nikoobakht and Mostafa A. El-Sayed. “Preparation and Growth Mechanism of Gold Nanorods (NRs) Using Seed-Mediated Growth Method”. In: *Chemistry of Materials* 15.10 (May 2003), pp. 1957–1962. ISSN: 0897-4756.

[13] Nicolas Bogliotti et al. “Optimizing the formation of biocompatible gold nanorods for cancer research: Functionalization, stabilization and purification”. In: *Journal of Colloid and Interface Science* 357.1 (2011), pp. 75–81. ISSN: 00219797.

[14] Armon Sharei et al. “A vector-free microfluidic platform for intracellular delivery.” In: *Proceedings of the National Academy of Sciences of the United States of America* 110.6 (Feb. 2013), pp. 2082–7. ISSN: 1091-6490.

[15] Jonathan N Rosen, Michael F Sweeney, and John D Mably. “Microinjection of zebrafish embryos to analyze gene function.” In: *Journal of visualized experiments : JoVE* 25 (Mar. 2009). ISSN: 1940-087X.

[16] Xavier Michalet. “Mean square displacement analysis of single-particle trajectories with localization error: Brownian motion in an isotropic medium.” In: *Physical review. E, Statistical, nonlinear, and soft matter physics* 82.4 Pt 1 (Oct. 2010), p. 041914. ISSN: 1550-2376.

[17] Thomas Bickel. “A note on confined diffusion”. In: *Physica A: Statistical Mechanics and its Applications* 377.1 (2007), pp. 24–32. ISSN: 03784371.

[18] H Qian, M P Sheetz, and E L Elson. "Single particle tracking. Analysis of diffusion and flow in two-dimensional systems." In: *Biophysical journal* 60.4 (Oct. 1991), pp. 910–21. ISSN: 0006-3495.

[19] Felipe Moser et al. "Cellular Uptake of Gold Nanoparticles and Their Behavior as Labels for Localization Microscopy." In: *Biophysical journal* 110.4 (Feb. 2016), pp. 947–53. ISSN: 1542-0086.

[20] Yingbo Zu et al. "Gold nanoparticles enhanced electroporation for mammalian cell transfection." In: *Journal of biomedical nanotechnology* 10.6 (June 2014), pp. 982–92. ISSN: 1550-7033.

[21] Juqiang Lin et al. "Rapid delivery of silver nanoparticles into living cells by electroporation for surface-enhanced Raman spectroscopy". In: *Biosensors and Bioelectronics* 25.2 (2009), pp. 388–394. ISSN: 09565663.

[22] Gregory Lee Szeto et al. "Microfluidic squeezing for intracellular antigen loading in polyclonal B-cells as cellular vaccines". In: *Scientific Reports* 5 (May 2015), p. 10276. ISSN: 2045-2322.

[23] S. Link et al. "Laser-Induced Shape Changes of Colloidal Gold Nanorods Using Femtosecond and Nanosecond Laser Pulses". In: *The Journal of Physical Chemistry B* 104.26 (July 2000), pp. 6152–6163. ISSN: 1520-6106.

[24] Stephan Link, Zhong L. Wang, and Mostafa A. El-Sayed. "How Does a Gold Nanorod Melt?" In: *The Journal of Physical Chemistry B* 104.33 (Aug. 2000), pp. 7867–7870. ISSN: 1520-6106.

[25] Marta Gordel et al. "Post-synthesis reshaping of gold nanorods using a femtosecond laser." en. In: *Physical chemistry chemical physics : PCCP* 16.1 (Jan. 2014), pp. 71–8. ISSN: 1463-9084.

[26] Peter Zijlstra, James W. M. Chon, and Min Gu. "White light scattering spectroscopy and electron microscopy of laser induced melting in single gold nanorods". In: *Physical Chemistry Chemical Physics* 11.28 (2009), p. 5915. ISSN: 1463-9076.

[27] Yukichi Horiguchi et al. "Photothermal Reshaping of Gold Nanorods Depends on the Passivating Layers of the Nanorod Surfaces". In: *Langmuir* 24.20 (Oct. 2008), pp. 12026–12031. ISSN: 0743-7463.

[28] E. O. Puchkov. "Intracellular viscosity: Methods of measurement and role in metabolism". en. In: *Biochemistry (Moscow) Supplement Series A: Membrane and Cell Biology* 7.4 (Dec. 2013), pp. 270–279. ISSN: 1990-7478.

[29] K. Fushimi. "Low viscosity in the aqueous domain of cell cytoplasm measured by picosecond polarization microfluorimetry". In: *The Journal of Cell Biology* 112.4 (Feb. 1991), pp. 719–725. ISSN: 0021-9525.

[30] R Swaminathan, C P Hoang, and A S Verkman. "Photobleaching recovery and anisotropy decay of green fluorescent protein GFP-S65T in solution and cells: cytoplasmic viscosity probed by green fluorescent protein translational and rotational diffusion." In: *Biophysical journal* 72.4 (Apr. 1997), pp. 1900–7. ISSN: 0006-3495.

[31] Kate Luby-Phelps. "The physical chemistry of cytoplasm and its influence on cell function: an update." In: *Molecular biology of the cell* 24.17 (Sept. 2013), pp. 2593–6. ISSN: 1939-4586.

[32] Katherine Luby-Phelps. *Microcompartmentation and Phase Separation in Cytoplasm*. Vol. 192. International Review of Cytology. Elsevier, 1999, pp. 189–221. ISBN: 9780123645968.

[33] Qian Peter Su et al. "Vesicle Size Regulates Nanotube Formation in the Cell." en. In: *Scientific reports* 6 (Apr. 2016), p. 24002. ISSN: 2045-2322.

[34] A Dupont et al. "Three-dimensional single-particle tracking in live cells: news from the third dimension". In: *New Journal of Physics* 15.7 (July 2013), p. 075008. ISSN: 1367-2630.